Coupled Two-Dimensional Computer Analysis of CW Chemical Mixing Lasers

ROBERT TRIPODI,* LAWRENCE J. COULTER,† BARRY R. BRONFIN,‡ AND LEONARD S. COHEN§
United Technologies Research Center, East Hartford, Conn.

The advantages of utilizing chemical reactions to support laser emission have been recognized for several years. However, a central problem identified in a variety of *cw* chemical mixing lasers is the dominance of gas-dynamics on the character of the flowing active medium, pointing to the need for a theoretical model that couples the effects of fluid mechanics of mixing with the nonequilibrium kinetics and the cascade of vibrational-rotational laser transitions. As one of the efforts to meet this need, a two-dimensional, rate equation model has been developed. A detailed discussion of the computer model is presented, as well as sample calculations for a representative "cold reaction" HF laser. Comparisons are made with experiment where appropriate.

Nomenclature

C_k = mass fraction of species k
c_p = specific heat at constant pressure
D_k = laminar diffusion coefficient for species k
ΔE_j = activation energy for reaction j
E_r = rotational-state energy
E_v = energy stored in vibrational state v
ΔE_v = $(E_{v+1} - E_v)$
g_v = optical gain coefficient for the transition $v+1 \rightarrow v$
g_o = threshold gain
h = Planck's constant, specific enthalpy
$\hat{h}$ = specific total enthalpy including heats of formation
h_k = specific enthalpy of species k
Δh_k = heat of formation for species k
ΔH_j = heat of reaction for reaction j
k = Boltzmann's constant, chemical rate coefficient, thermal conductivity
K = V-T or V-V rate coefficient
L = active optical path length
Le = Lewis number = $(D_k+\varepsilon_d)/(k+\kappa)$
m = velocity ratio between primary and secondary
$\dot{m}$ = mass flow rate
m_k = mass of one molecule of species k
M = Mach number
n = density ratio between primary and secondary
n_k = number density of species k
n_v = number density of emitter molecules in vibrational state v
$n_{v,J}$ = number density of emitter molecules in vibrational state v and rotational state J
p = pressure
p_o = total pressure
P_r = Prandtl number = $c_p(\mu+\varepsilon)/(k+\kappa)$
q = volumetric rate of heat addition to the gas mixture
q_{rad} = volumetric rate of radiative energy emission
Q_{rot} = rotational partition function
R = specific gas constant
$R_{v,v+1}$ = matrix element for the radiative transition $v+1 \rightarrow v$
r_1, r_2 = reflectivities of left and right mirrors
t = time
T = static temperature
T_o = total temperature
u = velocity in x (flow) direction
$\langle u \rangle$ = average relative velocity between molecules
v = velocity in z (transverse) direction
w_k = mass rate of production of species k per unit volume
W_v = intracavity flux (sum of right and left running fluxes) for the radiative transition $v+1 \rightarrow v$
X_i = dummy symbol for chemical species i
x = coordinate in flow direction
z = coordinate transverse to flow in optical direction
α_p = pressure-broadened half width
α_D = Doppler-broadened half width
$\alpha_{ij}, \alpha'_{ij}$ = stoichiometric coefficients for species i in reaction j
ε = eddy viscosity
ε_d = eddy diffusion coefficient
η = efficiency
κ = eddy thermal conductivity
μ = coefficient of viscosity
ν = frequency of emitted radiation
ξ = line shape parameter = $\alpha_p(ln2)^{1/2}/\alpha_D$
ρ = gas density
σ = specific power
ϕ = line shape factor

Presented as Paper 74-224 at the AIAA 12th Aerospace Sciences Meeting, Washington D. C., January 30–February 1, 1974; submitted April 5, 1974; revision received November 6, 1974. Work supported in part by the Advanced Research Projects Agency, monitored by the Air Force Weapons Laboratory, Kirtland AFB, New Mexico under Contract F29601-72-C-000.

Index categories: Lasers; Reactive Flows; Thermochemistry and Chemical Kinetics.

* Research Engineer, Nonequilibrium Chemistry Research.
† Supervisor, Engine Performance Group. Member AIAA.
‡ Principal Scientist, Nonequilibrium Chemistry Research.
§ Chief, Airbreathing Propulsion. Associate Fellow AIAA.

Introduction

IN a typical cw chemical laser, a primary reactant flow (e.g., F atoms for an HF laser) is supplied from a plenum through a group of nozzles where it is brought into contact with a secondary reactant in an injection/mixing region within the laser cavity. The mixing and subsequent chemical reactions produce a vibrationally excited reactant that can be stimulated to emit laser radiation.

As an aid in understanding and designing lasers of this type, analytical models have been developed to predict their performance. Among the first of these were quasi-one-dimensional models applicable to Fabry-Perot cavities.[1,2] Mixing effects were ignored and properties transverse to the flow direction were considered uniform. A more elaborate model was developed by Hofland and Mirels[3,4] wherein mixing proceeds by diffusion in a constant pressure environment. That model is limited by the imposition of the flame sheet approximation and total saturation of the medium. A subsequent numerical approach by King and Mirels[5] eliminated the flame sheet restriction, but was only truly applicable to amplifier configurations; turbulent mixing was not included in the model. Recently, more sophisticated two-dimensional mixing models have been developed that are applicable to laser oscillators. Among these are the Lockheed LAMP computer code[6] and the subject of the present work, the MIXLAS code developed at United Aircraft Research Labs. (UARL).[7]

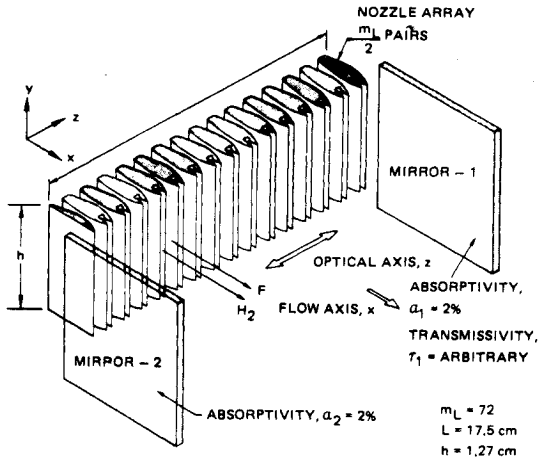

Fig. 1 Cavity schematic and coordinate system.

Description of the MIXLAS Analysis

The MIXLAS computer code was developed as a part of a comprehensive package of programs designed to characterize chemical lasers from the combustion chamber through the laser cavity. The intent of the effort was to make use of proven existing programs in a modular form with a minimum of actual modification of the programs except for the interfacing of one program with another. In keeping within these ground rules, a package of subroutines was added to the existing mixing-combustion program (MIX) to separately handle the details of chemical reactions, vibrational relaxation, and stimulated emission and feed this information to the mixing analysis as needed. The formulation assumes two-dimensional flow with parallel mixing; the pressure transverse to the flow at a given station is considered uniform. The model is applicable to Fabry-Perot laser cavities. A sketch of a representative geometry is given in Fig. 1.

Among the equations used to describe a two-dimensional chemical mixing laser analysis are the usual boundary-layer equations for two-dimensional reacting flows[8] with the Lewis and Prandtl numbers set equal to unity. These comprise the continuity equation

$$\frac{\partial \rho u}{\partial x}+\frac{\partial \rho v}{\partial z}=0 \tag{1}$$

the species continuity equation

$$\rho u\frac{\partial C_k}{\partial x}+\rho v\frac{\partial C_k}{\partial z}=\frac{\partial}{\partial z}\left[(\mu+\varepsilon)\frac{\partial C_k}{\partial z}\right]+w_k \tag{2}$$

the momentum equation

$$\rho u\frac{\partial u}{\partial x}+\rho v\frac{\partial u}{\partial z}=-\frac{dp}{dx}+\frac{\partial}{\partial z}\left[(\mu+\varepsilon)\frac{\partial u}{\partial z}\right] \tag{3}$$

the energy equation

$$\rho u\frac{\partial h}{\partial x}+\rho v\frac{\partial h}{\partial z}=\frac{\partial}{\partial z}\left[(\mu+\varepsilon)\frac{\partial h}{\partial z}\right]+q \tag{4}$$

where the mixture specific enthalpy is given by

$$h=\sum_{k=1}^{s} C_k\left[\int c_p dT\right]+\frac{u^2}{2} \tag{5}$$

and q represents the rate of heat addition to the gas from chemical reactions, vibrational deactivation,¶ and laser emission. Also included is the equation of state, $p=\rho RT$.

¶ Each HF vibrational state is treated as a separate species with an internal energy including its vibrational energy. Consequently the specific heat for each HF pseudo species is that appropriate to the translational and rotational modes only. The energetics of vibrational energy transfer are treated in the same manner as energy exchange in chemical reactions.

Any of a number of formulations for the eddy (turbulent) viscosity may be employed at user option. Models proposed by Cohen[9-11] and Ghia et al.[12] have been successfully applied to the prediction of turbulent variable-density, ducted flows. Until reliable formulations applicable to transitional flows are available they may be applied with modifications to such flows also. The formulation we most often use is that of Cohen, based upon a model developed by Görter.[13] The eddy viscosity may be described by the relationship

$$\varepsilon=C_1 b\rho u_{\mathfrak{L}}|1-m|\left(\frac{1+n}{2}\right)^{0.8} \tag{6}$$

where m is the velocity ratio between primary and secondary streams (centerline), n is the corresponding density ratio, b is the mixing height, and C_1 is a universal constant in each region of a mixing jet flow. ($C_1=0.00764$ in the core region of a two-dimensional flow and 0.0136 in the developed region.) As a flow preceeds downstream, and the velocity ratio m approaches unity, the eddy viscosity will tend to diminish. As a device for maintaining the eddy viscosity at a minimum level in an attempt to reflect the turbulence originally existing in the flows prior to the initiation of mixing, a critical velocity ratio m' may be specified. For axial positions downstream of the point at which m reaches the value m' the following relation holds[9]:

$$\varepsilon=C_1 b\rho u_{\mathfrak{L}}|1-m'|\left(\frac{1+n'}{2}\right)^{0.8}\left[\left(\frac{1+n'}{1+n}\right)\left(\frac{1+nm}{1+n'm'}\right)\right] \tag{7}$$

where n' is the density ratio at the point where $m=m'$.

In keeping with a modular approach in the development of the model, chemical, relaxational, and laser-emission rate processes are decoupled from the boundary-layer equations. In any given step in the calculations the previous equations are solved with the production rate term w_k eliminated from the species continuity equation and the heat addition term q eliminated from the energy equation. Based upon solutions thus obtained, average production rates are calculated, and the species mass fractions existing at step i are modified according to the relationship

$$C_{k(i)}=C_{k(i-1)}+\Delta C_k \tag{8}$$

where

$$\Delta C_k=\frac{1}{\rho}w_k\,\delta t \tag{9}$$

δt is the time interval for the calculational step and

$$w_k=m_k\dot{n}_k \tag{10}$$

The modification in enthalpy over an interval has contributions from chemical reactions and laser emission. Thus we have

$$\Delta h=-\sum_k \Delta C_k\Delta h_k-q_{\text{rad}}\,\delta t \tag{11}$$

where

$$q_{\text{rad}}=\sum_{v=0}^{v-1} g_v W_v \tag{12}$$

From the new values of total enthalpy h and the species mass fractions C_k a new static temperature can be evaluated.

The expressions needed to evaluate the contributions to the species production rates $\dot{n}_k$ and intracavity flux W_v are summarized. The rate of production of per unit volume can have several contributions. Chemical production of species k by r different reactions involving a species is represented by

$$\dot{n}_k|_{\text{chem}}=\sum_{j=1}^{r}(\alpha_{ij}-\alpha'_{ij})\left[k_{f_j}\prod_{l=1}^{s}(n_l)^{\alpha_{ij}}-k_{r_j}\prod^{s} n_l^{\alpha'_{ij}}\right] \tag{13}$$

where α_{ij} and α'_{ij} are stoichiometric coefficients in the chemical balance equation

$$\sum_{i=1}^{s}\alpha_{ij}X_i \underset{k_{r_j}}{\overset{k_{f_j}}{\rightleftharpoons}} \sum_{j=1}^{s}\alpha'_{ij}X_i \tag{14}$$

The rate coefficients are considered to be of Arhennius form[14]

$$k_{f_j}=aT^b\exp(-\Delta E_j/RT) \tag{15}$$

$$k_{r_j}=cT^d\exp(-(\Delta E_j-\Delta H_j)/RT) \tag{16}$$

In the case of the vibrational pseudo-species, the internal production rate can include V-T and V-V relaxation effects as well as radiative emission. Suppose that pseudo-species k represents the vibrational state v of the laser active species. Then the V-T contribution to the production rate is, in general

$$\dot{n}_k|_{V-T} = \dot{n}_v|_{V-T} = K_{v+1,v}[n_{v+1} - \exp(-\Delta E_v/kT)n_v] - K_{v,v-1}[n_v - \exp(-\Delta E_{v-1}/kT)n_{v-1}] \quad (17)$$

The rate coefficients are of Landau-Teller form [15,16] with modifications to account for anharmonicity. An exception is HF self deactivations, which has an unusual temperature dependence[17] and is stored as a table vs temperature. Also in the case of HF lasers, multi-quanta transitions resulting from interactions with H atoms are included based on the theoretical findings of Wilkins.[18] In that case terms representing transitions to nonadjacent states are included in the previous equation.

The production rate contribution from V-V transitions is represented by

$$\dot{n}_k|_{V-V} = \dot{n}_v|_{V-V} = \sum_{v'} K^{v'-1,v'}_{v+1,v}\{n_{v+1}\, n_{v'-1} - \exp[(\Delta E_v - \Delta E_{v'-1})/kT] n_v\, n_{v'}\} - \sum_{v'} k^{v_1 v'+1}_{v_1 v'-1} \times \{n_v\, n_{v'} - \exp[(\Delta E_{v-1} - \Delta E_{v'})/kT] n_{v-1}\, n_{v'+1}\} \quad (18)$$

Here the rate coefficients are treated in a form proposed by Rapp and Englander-Golden[19]

$$K^{v',v'-1}_{v,v+1} = v^1(v+1)\, K^{10}_{01} \operatorname{sech}^2(\alpha|\Delta E_v - \Delta E_{v'-1}|/\langle u\rangle) \quad (19)$$

The rate of change of population of a vibrational pseudo-species due to radiative transitions is given by

$$\dot{n}_k|_{\text{rad}} = \dot{n}_v|_{\text{rad}} = \frac{g_v W_v}{h\nu_v} - \frac{g_{v-1} W_{v-1}}{h\nu_{v-1}} \quad (20)$$

The line center gain coefficient g_v for the P-branch transition $v+1 \to v$, $J+1 \to J$ may be expressed as

$$g_v = \frac{8\pi^3}{3\pi}\phi J |R_{v,v+1}|^2 \left[\frac{n_{v+1,J-1}}{2J-1} - \frac{n_{v,J}}{2J+1}\right] \quad (21)$$

The rotational mode is taken to be in equilibrium with translation such that

$$n_{v,J} = \frac{n_v \exp[-E_r(v,J)/T]}{Q_{\text{rot}}} \quad (22)$$

For radiative lines in which both Doppler and pressure broadening are important the line-shape function ϕ is characterized by a Voigt profile[20]

$$\phi = \left(\frac{m}{2\pi kT}\right)^{1/2} e^{-\xi^2} erfc(\xi) \quad (23)$$

where

$$\xi = (\alpha_p/\alpha_D)(\ln 2)^{1/2} \quad (24)$$

The magnitude of the intracavity flux is evaluated based upon an extension of Rigrod's analysis[21] for transverse Fabry-Perot cavities under the assumptions of geometric optics and steady-state homogeneous radiative transitions, without consideration of any cavity modes. Since rotational equilibrium is assumed, predicted laser emission in each vibrational band is allowed to occur only on the P-branch exhibiting maximum gain. The approach followed is consonant with treatments previously developed by Hall and Bronfin[2] and Emanuel[1] for quasi-one-dimensional models.

To support laser emission, the gain in the propagation direction must be sufficient to balance losses to the mirrors. If the spatially averaged gain is less than this threshold value ($g_o = -\ln(r_1 r_2)/2L$) no emission will occur.[22] If collisional rate processes tend to drive the gain to a value higher than g_o the intracavity flux will be of such a magnitude to drive the average gain to the threshold value ($\int g_v\, dz/L = g_o$). To effect calculations describing these phenomena the gain on a transition is monitored until its value exceeds g_o. The approximation is made that the gain variation along the optical direction (z) may be prescribed. Preliminary estimates of the gain distribution are obtained by evaluating the unloaded gain for the x interval of interest, starting with the loaded gain values from the previous interval. The loaded gain distribution then is approximated by multiplying the unloaded gain by a factor that reduces the average to g_o. The difference between the unloaded values and the scaled values is then used to evaluate the energy given up to radiative processes and subsequently the intracavity flux. The effect of this approximation is to relax the usual constraint that the intracavity flux remains constant. Once an average flux value is found, however, it may be used to re-evaluate the loaded gain distribution for the interval. Iterations can be performed but they generally have been found to be unnecessary.

In the general calculational scheme the mixing equations are solved over each interval in the manner of an initial value problem wherein conditions at the end of one segment (appropriately modified by the detailed kinetics calculations) become the initial values for the next segment. This procedure is, of course, not strictly correct since the species production and heat addition terms should be directly coupled with the gas-dynamic conservation equations. While this technique tends to avoid mathematical instabilities, it might be at the expense of accuracy. To avoid this, tests are incorporated in the solution procedure that anticipate temperature changes over a given interval and restrict the step size to keep such a change within an arbitrarily specified limit. It has been found that limiting the maximum relative temperature change over an interval to 2% is usually sufficient to avoid serious numerical error. A reduction of this tolerance to 1% resulted in differences of less than 2% in all pertinent variables for the cases considered following.

Results

Description of Input

To demonstrate the capabilities of the model it was decided to base the input upon an experiment that conforms as nearly as possible to the constraints on the model (two-dimensional flow, flat mirrors), and also that is readily available in the literature. Consequently, early work of Spencer et al.[23,24] at Aerospace Corporation has been used for the test case.

The case of interest in an HF chemical laser** in which the reaction

$$F + H_2 \to HF(v) + H, \qquad v = 0,1,2,3$$

generates the excited HF molecules required for laser emission. The necessary F atoms are generated in a plenum by mixing arc heated nitrogen and SF_6 such that the mixture temperature is in excess of 2000K. At these temperatures the SF_6 dissociates, with F atoms among the products. The nitrogen, fluorine atoms, and the other dissociation products are then expanded through a series of two-dimensional primary nozzles to the entrance of the laser cavity. At that point, hydrogen gas is injected between the nozzles parallel to the primary streams (see Fig. 1). The H_2, emitted from perforations in tubes located at the nozzle exit plane and held transverse to the flow, expands to fill the base region and match the pressure of the primary. From this, the hydrogen molecules and the fluorine atoms mix and react to form vibrationally excited HF, which subsequently emits a part of its internal energy as laser radiation.

The experimental configuration is comprised of an array of 36 primary (fluorine) nozzles, each separated by a small base containing the hydrogen injectors. The overall nozzle and injector exit area exhausting to the cavity is approximately $\frac{1}{2}$ in. by 7 in. The optical path is along the 7 in. dimension transverse to the flow axis. The nominal flow conditions for the base case are as follows: $\dot{m}(N_2) = 6.9$ g/sec, $\dot{m}(SF_6) = 1.0$ g/sec, $\dot{m}(H_2) = 1.0$ g/sec; $p_o = 1.36$ atm, $T_o \simeq 2300$K. The nominal free jet conditions just prior to the hydrogen injection are: $T = 440$K, $p = 3.75$ torr, $M = 4.5$.

A stable plano-concave optical cavity was utilized, comprised of 2 in. diam. gold-plated berryllium copper mirrors with estimated reflectivity at the laser wavelengths of ~99%. Laser

** The model may also be employed to describe other chemical laser systems such as HCl and CO.

Table 1 Summary of results for base case[a]

Milestone	Start of laser emission	50% of total power	63% of total power	95% of total power	Laser cutoff
x-position (cm)	0.048	0.48	0.64	1.38	1.93
Degree of reaction	0.023	0.414	0.520	0.848	0.960
$\sigma_{10}(j/g)$	...	16.26	20.72	32.20	33.66
$\sigma_{21}(j/g)$	...	19.28	24.23	37.38	40.13
$\sigma_{32}(j/g)$	...	3.74	4.53	4.76	4.76
$\sigma_{tot}(j/g)$	...	39.27	49.48	74.32	78.54
Chemical heat addn (j/g)	6.81	122.82	154.41	251.61	284.93
Local efficiency, $\eta_L(\%)$	...	32.0	32.0	29.5	27.6
Overall efficiency, $\eta(\%)$	...	13.2	16.7	25.0	26.4

[a] Local efficiency $\eta_L \equiv 100\sigma_{tot}/$(chemical heat addn.); overall efficiency $\eta \equiv 100\sigma_{tot}/$(maximum heat addn.); maximum heat addn. = 296.96 j/g.

power was extracted through a uniform array of holes in the plane mirror. The concave mirror had a radius of curvature of 12 ft. and was positioned with a 3-ft separation from the plane reflector.

For the numerical calculations an element of the cavity geometry extending from the centerline of a fluorine nozzle to the centerline of an adjacent hydrogen injector is treated. (There are 72 repetitions of such an element within the actual cavity.) A plenum temperature of 2220K was used to evaluate the relative amounts of fluorine atoms and other products at thermochemical equilibrium in the heated SF_6-N_2 mixture. To match the nominal mass flows, boundary-layer effects could not be neglected in the nozzles. The computer program, however, cannot easily handle zero or small velocities. Consequently the velocity profile was faired to approximate the effects of boundary layers near the nozzle walls of sufficient thickness to match the specified mass flows. Since nonzero velocities must be utilized in the computer input, the entrance flow profile can be thought of as one representative of a point slightly downstream of the nozzle exit plane. As further approximations in setting up the input, the effects of heat transfer to the nozzle walls and the effect of the walls on local gas composition have been ignored. In the primary, a total temperature of 2220K is assumed along with mass fractions for the constituents as follows: F, 0.0482; N_2, 0.8734; S, SF_4 etc., 0.0784. In the secondary, which is comprised entirely of H_2, a total temperature of 540K is used. Possible consequences of the assumption of uniform total temperature and composition will be discussed later. The input velocity profile is shown in Fig. 2.

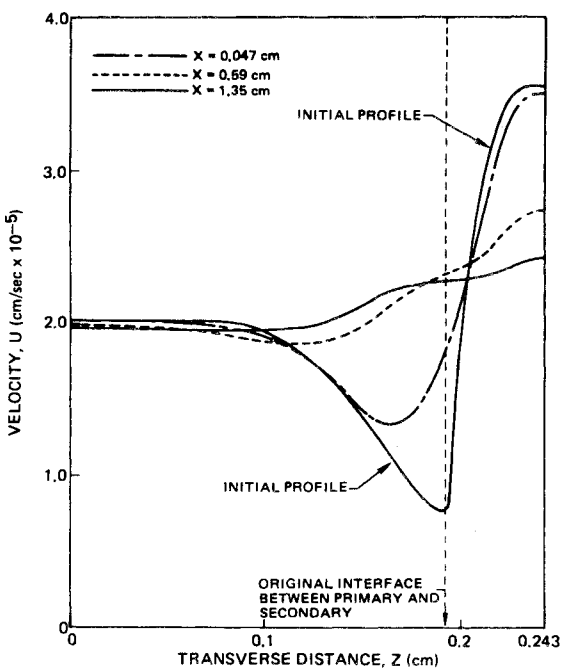

Fig. 2 Transverse velocity profiles.

In the treatment of the various rate processes, the physiochemical data employed is derived primarily from the values suggested by Cohen,[17] supplemented by the multiple quanta V-T transfer data for collisions with H atoms as given by Wilkins.[18] By-products of the SF_6 dissociation, other than fluorine, are grouped together and treated as one chemically inert species, which is assumed to deactivate vibrationally excited HF at the same rate as N_2. Also, the vibrational state of the N_2 is taken to be frozen throughout the flow.

Although the actual experiment utilized a stable plano-concave optical resonator, that cavity must be approximated as a plane-wave Fabry-Perot cavity free of geometric modes for the purposes of the calculation. Each reflector is assumed to have an absorption coefficient at the laser wavelengths of 2%. The transmissivity of the output mirror is taken to be equal to the percent open area taken up by the holes in the flat mirror. As a base case an equivalent transmissivity of 15% was used.

For all cases, the Cohen formulation of the eddy viscosity was used. Based upon previous experience running MIXLAS with nozzles similar in size to those for these cases a value for the maximum allowed velocity ratio m' of 0.8 was selected. Such a value implies that a small, but nonnegligible amount of turbulence did exist in the flow at the cavity entrance and would persist throughout the flow.

Results for Base Case

The results of the base case calculation are summarized in Figs. 2–11 and in Tables 1 and 2. Figure 2 represents the

Table 2 Energy balance for cw HF combustion-mixing laser (15% transmissivity)

Output	σ (j/gm)	η (%)
Laser emission (transmitted)		
$3 \rightarrow 2$	3.85	1.3
$2 \rightarrow 1$	31.48	10.6
$1 \rightarrow 0$	26.43	8.9
Subtotal	61.76	20.8
1) Mirror heating ($\alpha_i = 2\%$; $\tau = 15\%$)	17.00	5.7
2) V-T relaxation	44.71	15.1
3) Direct chemical heating of translation and rotation	85.55	28.8
4) Residual vibrational excitation [$HF(v)$] convected away:	76.12	25.6
5) Residual chemical potential [$F\cdot$, $H\cdot$] convected away:	11.82	4.0
Total	296.96	100.0

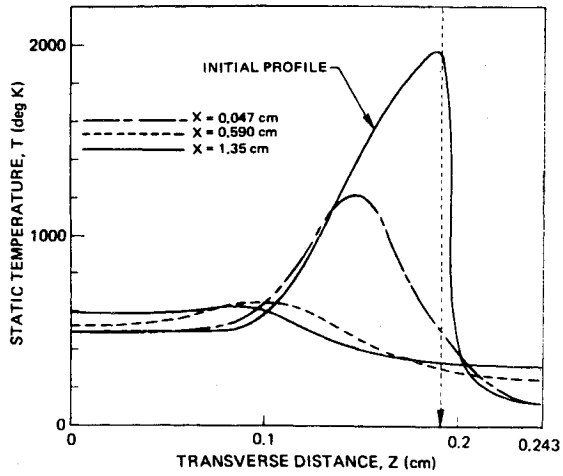

Fig. 3 Transverse temperature profiles. Vertical dashed line in this and subsequent figures indicates position of original interface between primary (on left) and secondary (on right) flows.

predicted evolution of the velocity profile as the flow progresses downstream. Four profiles are shown: the initial profile; the profile at $x = 0.047$ cm., near the start of laser emission; at $x = 0.59$ cm. near the point where 63% (the fraction $1 - 1/e$) of the laser power has been extracted; and at $x = 1.34$ cm., near the point where 95% of the laser power has been extracted. Note that the initial depression in the profile in the vicinity of the nozzle wall washes out fairly rapidly, but is still evident at the 63% power point.

Figure 3 represents the evolution of the static temperature profile as the flow progresses downstream. Profiles are shown at the same x positions as for Fig. 2. In conjunction with the input velocity profiles and the assumed total temperatures at the nozzle walls the temperature is initially quite high near the interface between primary and secondary ($z = 0.192$ cm). Had heat transfer to the walls been accounted for, this peak temperature would have been somewhat lower. As the gases mix and the lower velocity region is accelerated the temperature peak diminishes and shifts towards the primary flow. Note that after the peak has been eliminated (beyond $x = 0.59$ cm) the temperature levels are not much higher than the original core-flow temperatures. This relatively smooth temperature variation is a consequence of the high diluent levels used.

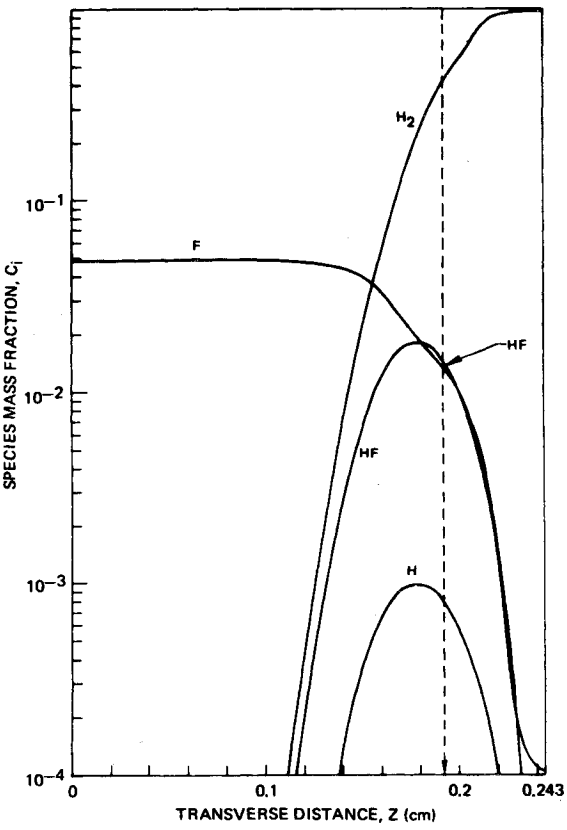

Fig. 4 Transverse reactant profiles; $x = 0.047$ cm, the start of lasing zone.

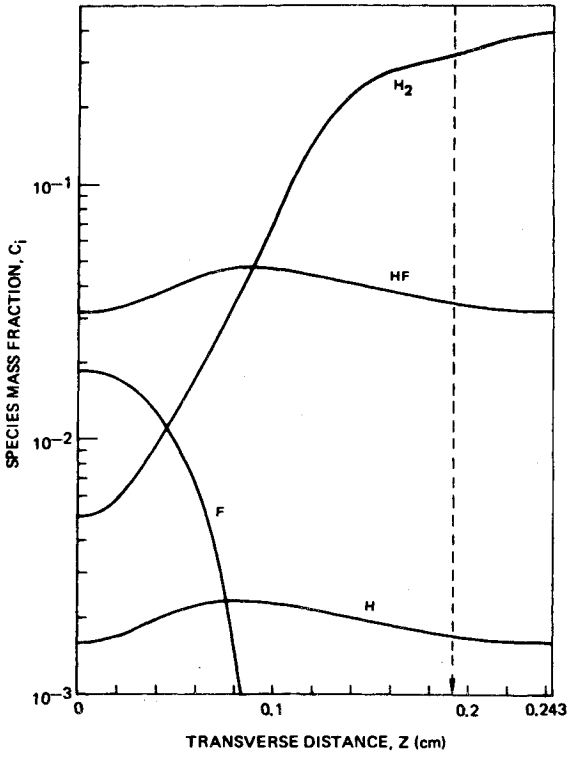

Fig. 5 Transverse reactant profiles; $x = 1.34$ cm, the 95% power point.

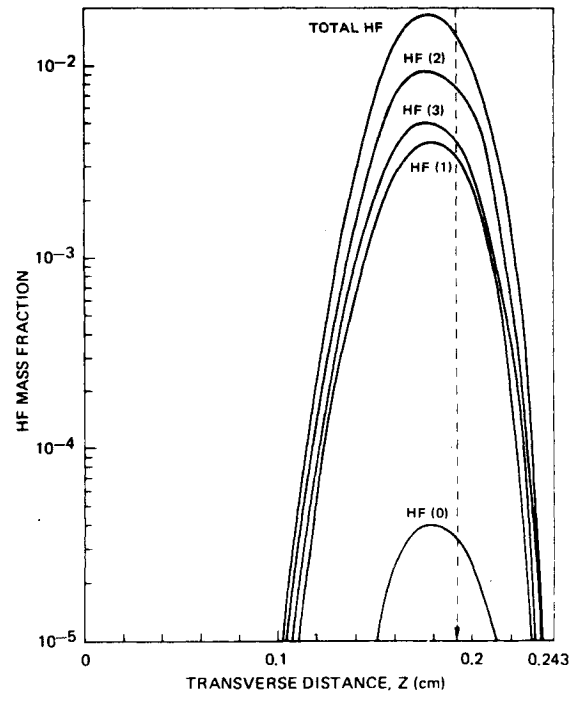

Fig. 6 Transverse HF vibrational distribution; $x = 0.047$ cm.

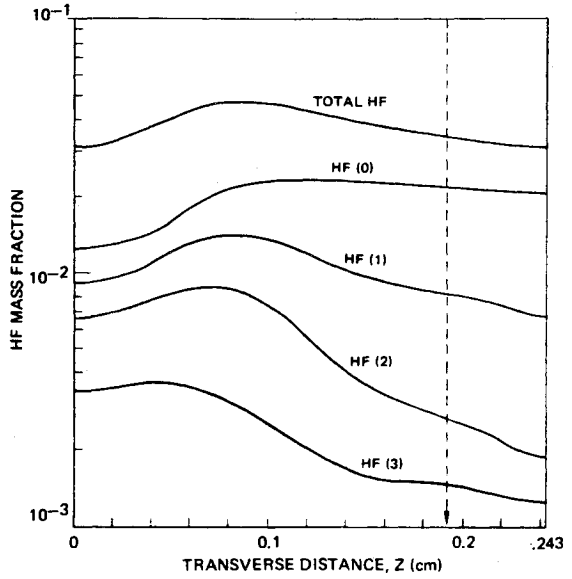

Fig. 7 Transverse HF vibrational distribution; $x = 1.34$ cm.

Figures 4 and 5 illustrate transverse species distribution profiles calculated for a point near the start (0.047 cm) and near the end (1.59 cm) of the lasing zone. At first the chemical production of HF is centered near the transverse position ($z = 0.192$ cm) corresponding to the initial division between primary and secondary. As the hydrogen intrudes further and further into the fluorine stream, the region of maximum HF production shifts in that same direction. The effects of this shift are illustrated, to some extent, in Figs. 6 and 7, which show the distribution of HF over important vibrational states at the same locations as the two previous figures. Note that at $x = 0.047$ cm (Fig. 6) the distribution over vibrational states closely approximates the pumping distribution of newly formed HF since neither relaxation nor laser emission has yet had a significant effect. By $x = 1.34$ cm, however, only partial population inversions are predicted. Note that towards the left of Fig. 7 the vibrational level populations are more closely grouped than at the right, because the HF in that region is more recently formed and has not been as severely deactivated as the "older" HF formed near the original primary-secondary interface. By this x location, the HF production reactions are 85% complete. Subsequent production of HF proceeds at a slower rate, such that deactivation completely dominates chemical pumping in the upper levels. This competition is best illustrated by Fig. 8, which shows axial species variations. Note that the population of HF ($v = 3$) starts diminishing only one cm downstream from the nozzle exit plane.

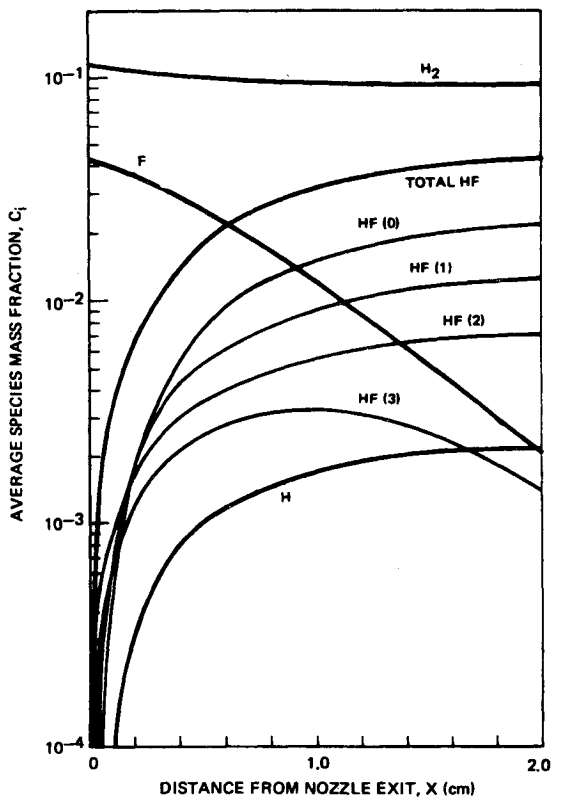

Fig. 8 Axial reactant variation.

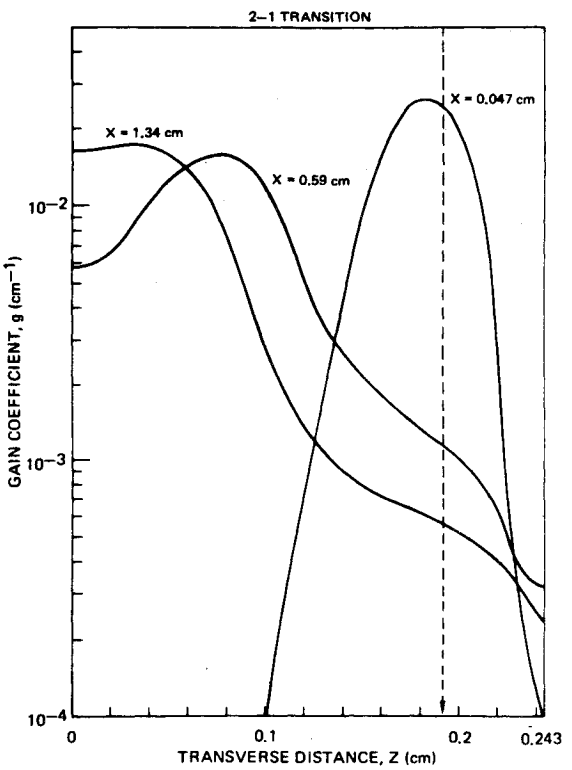

Fig. 9 Transverse gain distribution; 2–1 transition.

Of particular interest in the study of chemical lasers are the parameters directly related to laser performance, such as gain, intracavity flux, and specific power. Figure 9 illustrates the transverse gain profiles in the presence of laser flux for a sample transition ($v = 2 \rightarrow v = 1$) at the axial locations corresponding to laser initiation and the 63% and 95% power points. Since the condition is enforced that the spatially averaged gain along the cavity axis equals the threshold value as long as there is laser emission, each profile has the same average (0.0057 cm^{-1} for this case). Note the migration of the peak gain region to the left into the F-rich flow as the production of excited HF moves left while older HF presisting to the right becomes depleted by deactivation.

Figures 10 and 11 illustrate the development of the intracavity flux and specific laser power as the flow progresses downstream. Table 1 summarizes the development of laser power for the different transitions at various axial stations in the cavity. Table 2 describes predicted fate of all the available chemical energy at the point where laser emission ceases. The laser is seen to be quite efficient. At laser cutoff more than 26% of the maximum possible energy that could be added to the gas by chemical reactions††

†† In evaluating the maximum possible chemical heat addition it is assumed that all the available free F atoms (4.25% of the gas by weight) react to form HF. None of the F atoms included in other products of the SF_6 dissociation (e.g., SF_4) are assumed to take part in reactions in the laser cavity.

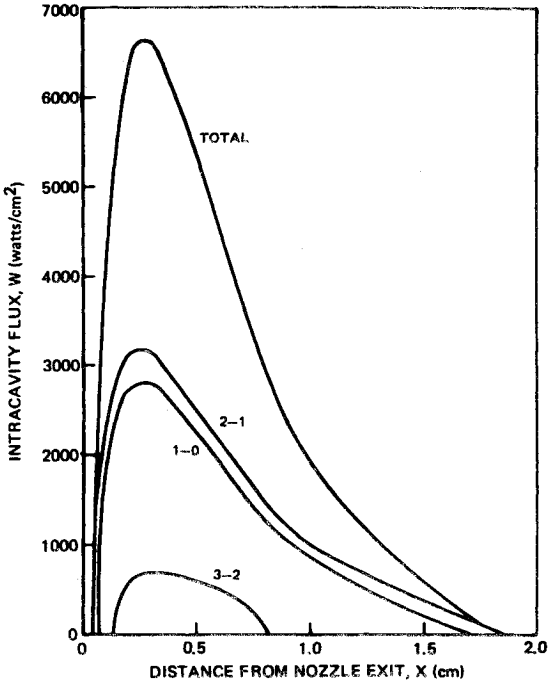

Fig. 10 Intracavity flux development.

has been extracted by radiative emission (although some of that is absorbed by the mirrors). The primary reason for this high efficiency is the low concentrations of reactants in this very dilute active medium. In particular, the partial pressure of the rapid deactivators HF and H is low thereby minimizing the deleterious effect of V-T relaxation. For this case only 15% of the energy available to laser emission is lost to V-T decay. In the later stages of the flow, however, it can be seen that V-T relaxation does degrade performance as the locally defined efficiency (see Table 1) tends to decline with increasing distance downstream.

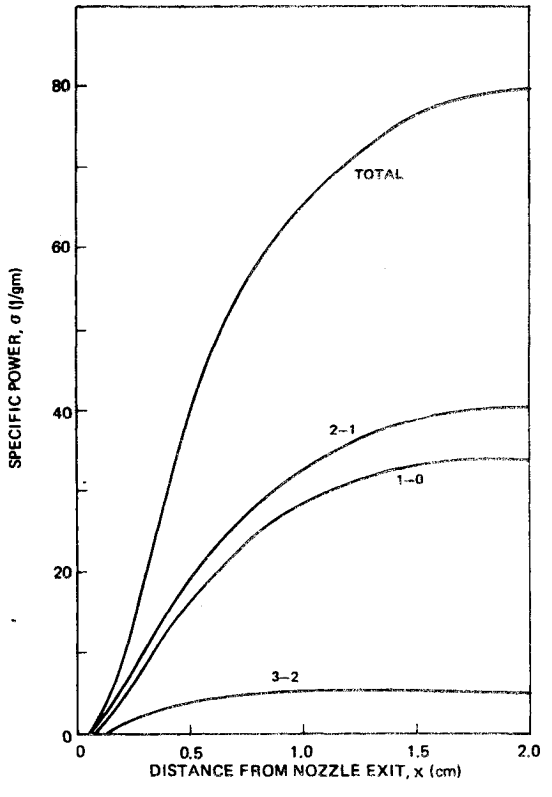

Fig. 11 Specific power growth.

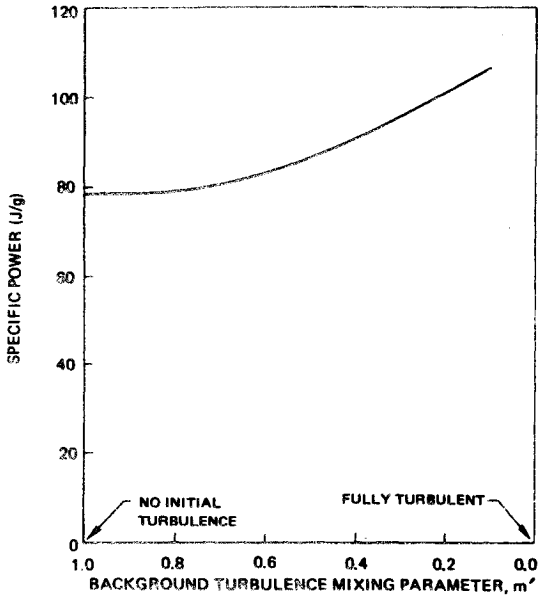

Fig. 12 Dependence of laser power on mixing parameter m'.

In high-power devices the effects of V-T deactivation can be more pronounced due to the generally higher concentrations of HF and H, and also often due to the presence of DF used to generate F atoms chemically in the combustion chamber. In such combustion driven devices, highly deactivated HF formed early in the flow can seriously limit the amount of energy that can be extracted from HF formed later on.

Effects of Rate of Mixing

With a computer code to describe the performance of a chemical mixing laser available, it is natural to evaluate the effect upon performance of the rate of mixing. Such a study was done for the base case. In the calculations previously described, the Cohen formulation to describe the eddy viscosity ε was employed [see Eqs. (1) and (2)]. In that formulation, a critical velocity ratio m' describes the point at which downstream preturbulence becomes dominant. Increasing values of m' represent decreasing amounts of preturbulence, and a generally decreased rate of mixing. A value of $m' = 1$ implies no initial turbulence so that as the velocity distribution becomes uniform the eddy viscosity will be eliminated completely.

The baseline calculations previously described were performed with $m' = 0.8$. Further calculations were performed varying m' from 1.0–0.1. The variation of the specific laser power with m' is plotted in Fig. 12. For higher values of the m' (i.e., 0.8–1.0) there is virtually no change in predicted performance. This insensitivity is partly due to the model employed for calculating the eddy viscosity, which in all cases regardless of m', the same value of ε is calculated until the point at which the true velocity ratio m reaches the value m'. Only beyond that point are differences in the mixing rate significant. For the cases presented here having high values of m', virtually all the lasing occurs before the critical point where $m = m'$ is reached. At lower specified values of m' the calculated eddy viscosity will remain higher longer and more rapid mixing will occur in the lasing zone. This more rapid mixing facilitates more rapid chemical reactions and enables more laser power to be extracted before deactivation mechanisms predominate. A perhaps more interesting study would be to vary the values of the constant C_1 (see Eq. 6) between 0 and it's normal value for a fixed m', thus covering the range from laminar to turbulent flow.

Comparison with Experiment

A theoretical model is useful only if it compares reasonably well with appropriate experiments, especially in predicting trends.

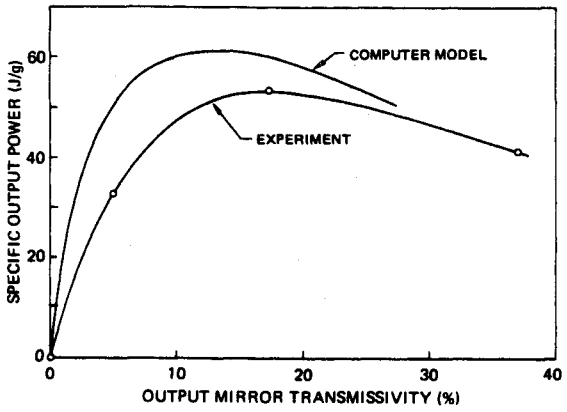

Fig. 13 Variation of output power with transmissivity; comparison with experiment.

Among the experiments performed by Spencer et al.[23] were studies of the effect of output mirror transmissivity (i.e., percent open area on the flat mirror) and injector mass flow rate on the transmitted power. These parameter studies were duplicated by the computer program. A value of $m' = 0.8$ was used throughout. The effect of varying the mirror transmissivity is illustrated in Fig. 13. It can be seen that the comparison between theory and experiment is reasonably good. Theory predicts slightly higher transmitted specific powers and a maximum at a lower transmissivity (14.5% vs 18.75%). The comparison for the variation of H_2 mass flow is also reasonably good. These results are shown in Fig. 14. The curves are normalized to the appropriate maximum power output (experimental maximum for the experimental curve and theoretical maximum for the theoretical curve). Note that the theoretical calculations tend to underestimate performance for low H_2 mass flows and overestimate it for high H_2 mass flows. The predicted optimum is also shifted slightly to a higher $\dot{m}_{H_2}$ than found experimentally. These results tend to indicate that deactivation by H_2 is more important than is assumed in the model (e.g., possible V-V interactions between H_2 and HF are not treated directly). Nevertheless, the comparison is quite encouraging, since the point of optimum performance is predicted closely.

Conclusions

A computer analysis has been developed that shows the potential for being a useful analytic tool in the study of *cw* chemical mixing lasers. Despite its limitations (e.g., Fabry-Perot optics only, two-dimensional mixing with no transverse pressure gradients) and the problems associated with finding experiments with reported conditions sufficiently defined to provide validation, this limited comparison with experiment previously described is encouraging.

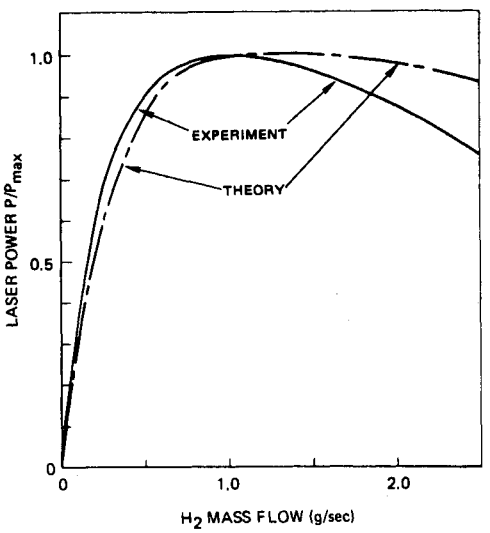

Fig. 14 Variation of output power with H_2 mass flow; comparison with experiment.

Primarily as a matter of convenience to facilitate program input, the effects of wall cooling and F-atom recombination in the nozzle were ignored. It is expected that inclusion of such effects would modify the results somewhat. For example, wall cooling would tend to reduce the temperature in the boundary-layer region, thus retarding the rate of chemical reactions and perhaps degrading laser performance. However, at the relatively high temperatures initially in the boundary layer, even a reduction of the peak temperature from 2000K–1500K causes only a 15% reduction in the kinetic rate of the dominant "cold" reaction ($F + H_2 \rightarrow HF + H$). A lowering to 1000K would result in less than a 35% reduction. Moreover the quantity of material contained within the boundary-layer region comprises only a fraction of the total mass flow (25% of the primary), whereas nearly all the flow (96%) has reacted by laser cut-off. Consequently it is felt that for these cases, inclusion of wall cooling effects would not have strongly affected the theoretical predictions. Similarly wall recombination effects are not expected to influence the results strongly. In any case the predictions would tend to imply somewhat poorer performance, bringing theory and experiment into closer agreement. A possibly significant assumption of the model is the neglect of transverse pressure gradients. The nonuniform heating of the gas due to chemical reactions can result in local variations in the transverse pressure. Higher pressure areas would tend to have enhanced chemical reaction and vibrational relaxation rates that could change the overall performance. Furthermore, significant pressure variations could lead to aerodynamic disturbances that could degrade performance. Fortunately, in the case previously described the maximum pressure variation is estimated to be less than 0.25 torr (6% of nominal pressure) and should not strongly affect the predicted result. In cases with lower diluent fractions, however, transverse pressure gradients can become important, and such effects should be treated. In addition basic understanding of mixing phenomena in transitional regimes is still needed for incorporation in the theoretical mixing model. Fabry-Perot optics are inadequate for describing accurately complex mode structure observed in cw chemical lasers. The understanding of what are appropriate kinetic models and the associated rate coefficients is incomplete. Current efforts are directed at addressing these problems.

Despite these limitations, however, the MIXLAS model does represent as advance over (and supplement to) commonly used quasi-one-dimensional models. Through the use of good engineering judgment and calibration with available experimental data, trends can be predicted and optimum performance bracketed. In addition some insight into the details of the interactions of kinetic and mixing processes in chemical lasers can be gleaned.

References

[1] Emanuel, G., "Analytical Model for a Continuous Chemical Laser," *Journal of Quantitative Spectroscopy and Radiative Transfer*, Vol. 11, 1971, pp. 1481–1520.

[2] Hall, R. J., Bronfin, B. R., Meinzer, R. A., and van den Bogaerde, J., "CW Combustion Mixing Chemical Laser: HF, DF," Proceedings of the *6th International Quantum Electronics Conference*, Kyoto, Japan, Sept. 1970.

[3] Hofland, R. and Mirels, H., "Flame-Sheet Analysis of CW Diffusion-Type Chemical Lasers, I. Uncoupled Radiation," *AIAA Journal*, Vol. 10, April 1972, pp. 420–428.

[4] Hofland, R. and Mirels, H., "Flame-Sheet Analysis of CW Diffusion-Type Chemical Lasers, II. Coupled Radiation," *AIAA Journal*, Vol. 10, Oct. 1972, pp. 1271–1280.

[5] King, W. S. and Mirels, H., "Numerical Study of a Diffusion-Type Chemical Laser," *AIAA Journal*, Vol. 10, Dec. 1972, pp. 1647–1654.

[6] Theones, J. and Ratliff, A. W., "Chemical Laser Oscillator Analytical Model," AIAA Paper 73-644, 1973, Palm Springs, Calif.

[7] Bronfin, B. R., Cohen, L. S., Coulter, L. J., McDonald, H.,

Shamroth, S., and Tripodi, R., "*Development of Chemical Laser Computer Models,*" Tech. Rep. AFWL-TR-73-48, July 1973, Air Force Weapons Laboratory, Kirtland AFB, New Mexico.

[8] Vasiliu, J., "Turbulent Mixing of a Rocket Exhaust Jet with a Supersonic Stream Including Chemical Reactions," *Journal of the Aerospace Sciences,* Vol. 29, Jan. 1962, pp. 19–28.

[9] Cohen, L. S., "A Kinematic Eddy Viscosity Model Including the Influence of Density Variations and Preturbulence," SP-321, *Free Turbulence Shear Flows, Vol. 1—Conference Proceedings,* July 1972, NASA.

[10] Cohen, L. S. and Guile, R. N., "Measurements in Free Jet Mixing/Combustion Flows," *AIAA Journal,* Vol. 8, June 1970, pp. 1053–1061.

[11] Bowman, C. T., Cohen, L. S., and Director, M., "Nitric Oxide Production in Combustion Processes with Strong Recirculation," EPA-R2-73-291, July 1973, Environmental Protection Agency, Washington, D.C.

[12] Ghia, K. N., Torda, T. P., and Lavan, Z., *Turbulent Mixing in the Initial Region of Heterogeneous Axisymmetric Coaxial Confined Jets,* CR-1615, May 1960, NASA.

[13] Görtler, H., "Berenchnung von Aufgaben der Freien Turbulnez auf Grand eines Neuen Naherungsansatzes," *Zeitschrift für angewandte Mathematik und Mechanik,* Vol. 22, 1942, pp. 244–254.

[14] Vincenti, W. G. and Kruger, C. K., *Introduction to Physical Gas Dynamics,* Wiley & Sons, New York, N. Y., 1965.

[15] Landau, L. and Teller, E., "Zur Theorie der Schalldispersion," *Physik Z. Sowjetunion,* Vol. 10, 1936A, pp. 34–47.

[16] Schwartz, R. N., Slawsky, J., and Herzfeld, K. F., "Calculation of Vibrational Relaxation Times in Gases," *Journal of Chemical Physics,* Vol. 20, pp. 1591–1599.

[17] Cohen, N., *A Review of Rate Coefficient Data for Reactions in the H_2-F_2 Laser System (Revised),* SAMSO TR 72-23, 1972, Aerospace Corp., El Segundo, Calif.

[18] Wilkins, R. L., "Monte Carlo Calculations of Reactions Rates and Energy Distribution Among Reaction Products II. $H + HF(v) \rightarrow H_2(v') + F$ and $H + HF(v) \rightarrow HF(v') + H$," *Journal of Chemical Physics,* Vol. 58, 1973, pp. 3038–3046.

[19] Rapp, D. and Englander-Golden, P., "Resonant and Near-Resonant Vibrational-Vibrational Energy Transfer Between Molecules in Collisions," *Journal of Chemical Physics,* Vol. 36, 1965, pp. 2487–2490.

[20] Armstrong, B. H., "Spectrum Line Profiles: the Voight Function," *Journal of Quantitative Spectroscopy and Radiative Transfer,* Vol. 7, 1967, pp. 61–88.

[21] Rigrod, W. W., "Saturation Effects in High-Gain Lasers," *Journal of Applied Physics,* Vol. 36, Aug. 1965, pp. 2487–2490.

[22] Marlow, W. C., "Approximate Lasing Condition," *Journal of Applied Physics,* Vol. 41, Sept. 1970, pp. 4019–4022.

[23] Spencer, D. H., Mirels, H., Jacobs, T. A., and Gross, R. W. E., "Preliminary Performance of a cw Chemical Laser," *Applied Physics Letters,* Vol. 16, 1970, pp. 235–237.

[24] Spencer, D. H., Mirels, H., and Jacobs, T. A., "Comparison of HF and DF Continuous Chemical Lasers: I. Power," *Applied Physics Letters,* Vol. 16, 1970, pp. 384–386.